science, engineering and health studies

Research Article

Science, Engineering and Health Studies
https://lio1.tci-thaijo.org/index.php/sehs
ISSN (Online): 2630-0087

Photodegradation of S-metolachlor using metal oxide doped tungsten oxide under visible light

Linda Horiean[1], Thanyaluck Sakonwaree[1], Nontaporn Sirichaiwattananun[1], Pramoch Rangsunvigit[2] and Mutsee Termtanun[1]*

[1] Department of Chemical Engineering, Faculty of Engineering and Industrial Technology, Silpakorn University, Nakhon Pathom 73000, Thailand
[2] The Petroleum and Petrochemical College, Chulalongkorn University, Bangkok 10330, Thailand

***Corresponding author**:
Mutsee Termtanun
termtanun_m@su.ac.th

***Received**: 24 June 2020*
***Revised**: 23 August 2020*
***Accepted**: 25 August 2020*
***Published**: 9 March 2021*

***Citation**:
Horain, L., Sakonwaree, T., Sirichaiwattananun, N., Rangsunviigit, P., and Termtanun, M. (2021). Photodegradation of S-metolachlor using metal oxide doped tungsten oxide under visible light. Science, Engineering and Health Studies, 15, 21040004.

ABSTRACT

In this research, tungsten oxide (WO_3) nanoparticles were modified by doping oxide of bismuth (Bi), vanadium (V), or manganese (Mn) at 0.5, 1, 2% (w/w). The undoped WO_3 and Bi/V/Mn oxide doped WO_3 were synthesized by using sol-gel method to find out the suitable metal loading amount for S-metolachlor degradation. After synthesis, the methods and techniques were performed for characterization the prepared catalysts. The photocatalytic activities of undoped and doped WO_3 samples in catalyzing S-metolachlor degradation under visible light were determined. After 4 h reaction, ultraviolet-visible (UV-Vis) spectroscopy was performed to observe the remaining concentration of S-metolachlor. From the characterization results, WO_3 had larger surface area and crystalline size after loading Bi/V/Mn oxide, but with the less electrons-holes recombination. Among three different doped metal oxides and different doping quantities, 1% (w/w) Bi_2O_3 doped WO_3 had the least electrons-holes recombination rate and provide the highest photocatalytic efficiency with 55.43% S-metolachlor degradation for a period of 4 h under visible light. Furthermore, the reusability of doped-photocatalysts was also examined to check the deactivation possibility. There was approximately 3% decrease in photoactivity of 1% (w/w) Bi_2O_3 doped WO_3 after repeating photodegradation of S-metolachlor for 3 times.

Keywords: photodegradation; tungsten (III) oxide; S-metolachlor; bismuth; vanadium; manganese

1. INTRODUCTION

The herbicide S-metolachlor has been used in more than 70 different crops in many agricultural sites since the 1970s (Long et al., 2014; Rosenfeld and Feng, 2011). Generally, the herbicide S-metolachlor was remained as toxic contaminate in ubiquitous groundwater and soil, since it is mainly used to control the broadleaf and grassy weeds (Long et al., 2014; Rosenfeld and Feng, 2011). It has high solubility of water (480 mg/L) at 20°C. However, it is normally difficult in for degradation by photolysis because of high half-life period (Rosenfeld and Feng, 2011). The removal of groundwater contaminants using advance oxidation processes (AOPs) seems to be one of potential options to reduce S-metolachlor to an acceptable range of contaminants (Badawy et al., 2006; Laoufi and Bentahar, 2014). Although titanium dioxide (TiO_2) is a conventional photocatalyst, it is working effectively within ultraviolet wavelength, but requires development to render more photoactivity under visible light. So far, many semiconductors have received much attention as they have abilities to compete with TiO_2, especially tungsten oxide (WO_3) which is initially applied as nitrogen dioxide (NO_2) gas sensor for air pollution treatment (Fraga et al., 2013). When WO_3 has a narrow band gap of 2.8 eV, it can absorb the light well in visible region (Wang et al., 2003). However, it has some

drawbacks due to its low stability, small surface area, and easy recombination of electrons and holes. Synthesis of WO_3 using sol-gel method offers high crystalline phase with low cost, simple procedure, and also suitable for industrial scale production (Susanti et al., 2014). This research aims to enhance the performance of WO_3 by doping with transition metal oxide such as bismuth oxide (Bi_2O_3), vanadiumoxide (V_2O_5), and manganese oxide (MnO_2), as they have advantages in enhancing surface area and stability, reducing band gap energy, and supporting charges separation in photocatalytic degradation of S-metolachlor under visible light.

2. MATERIALS AND METHODS

2.1. Materials and chemicals

Tungsten (VI) chloride ≥99.9% (Sigma-Aldrich, Singapore) was used for preparing a tungsten-based catalyst of undoped WO_3 and Bi/V/Mn oxide doped WO_3. Bismuth (III) chloride anhydrous 98% (Acros Organics, USA), vanadium (V) chloride 97% (Sigma-Aldrich, Singapore), and manganese (II) chloride tetrahydrate 99% (QRec, New Zealand) were used as precursors of metal oxide promoters. Ethanol 99.9% (RCL Labscan, Thailand) was used as solvent in metal precursor preparation. Silver nitrate 99.9% (POCH, Poland) and ammonia solution 25% (QRec, New Zealand), hydrogen peroxide 30% (QRec, New Zealand), and Triton-X 100 pure (AppliChem, Germany) were used in sol-gel technique. In photodegradation experiment, S-metolachlor 98% PESTANAL analytical standard (Sigma-Aldrich, Singapore) was used as a model herbicide.

2.2 Catalysts preparation

Each doped catalyst was prepared by adding tungsten (VI) chloride precursor with bismuth (III) chloride, vanadium (V) chloride, or manganese (II) chloride into ethanol and 0.5 M ammonia hydroxide. Then, they were mixed and stirred at the low temperature for 24 h. The mixture was then titrated with 0.1 M of silver nitrate and washed with deionized water and followed by centrifuging until no white silver chloride was appeared. Then, surfactant (Triton-X 100) was added into mixture and vigorously stirred to form a sol structure (Susanti et al., 2014). Then, the tungsten sol was placed in the oven at 60°C to dry overnight. The calcination temperature was at 450°C with a heating rate of 5°C/min and left in the autoclave until the gel was formed. Catalyst preparation procedure based on sol-gel method is shown in Figure 1.

2.3 Catalysts characterization

In this research, characterizations of various catalysts were performed using X-ray diffraction (XRD), nitrogen adsorption/desorption (BET), UV-visible spectroscopy (UV-Vis), X-ray fluorescence spectrometer (XRF), and photoluminescence spectrometer (PL). The crystal structures and phase compositions were analyzed by XRD using CuKα radiation between the 2 theta range of 20-80° with 2°/min. BET was performed at 4°C. The preheater was used to remove the moisture with helium flow of 50 mL/min at 150°C for 3 h, followed by the nitrogen adsorption step. UV-Vis was carried out at the absorption wavelength of 210 nm to measure the remaining concentration S-metolachlor. To measure the light absorption of all prepared WO_3, UV-Vis was carried out at the light wavelength between 190 nm and 900 nm. XRF was applied to confirm the loading amount of Bi/V/Mn oxide. The electrons-holes recombination rate of all WO_3 catalysts was determined using PL with the excitation wavelength at 380 nm.

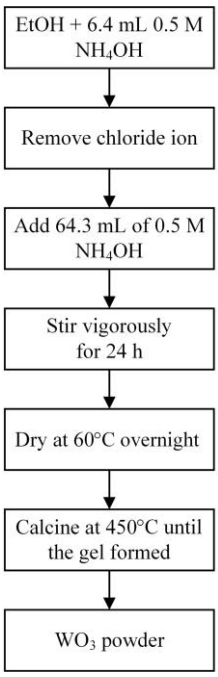

Figure 1. Photocatalyst preparation using sol-gel method

2.4 Photodegradation of S-metolachlor under visible light

The photoactivity measurements of prepared WO_3 catalysts in S-metolachlor photodegradation were performed in the black box using 4 numbers of 45 W fluorescent bulbs as light source (2450 lumen/lamp and wavelength around 620 nm). Two ventilation fans were used to keep ambient temperature constant. Initial concentration (5 ppm) of S-metolachlor was mixed with 0.5 g/L of prepared WO_3 for 4 h under visible light atmosphere. The photodegradation of S-metolachlor was determined by detecting the remaining concentration of S-metolachlor using UV-Vis. To neglect the influence of surface adsorption of S-metolachlor on prepared WO_3 catalysts, the mixed solution was left 30 min in dark atmosphere prior to the starting of each photocatalytic degradation experiment.

3. RESULTS AND DISCUSSION

3.1. Characterization results

The results of BET surface area of Bi/V/Mn oxide doped WO_3 and undoped WO_3 synthesized by sol-gel method are shown in Table 1. BET surface area of undoped WO_3 was equal to 18.77 m^2/g. Doping Bi/V/Mn oxide on WO_3 led to an increase in the surface area in the order of Bi>V>Mn. MnO_2 (0.5% w/w) doped WO_3 showed the highest surface area at 32 m^2/g. However, the surface area of catalysts decreased as loading amount of metal oxide is increased since it may cause agglomeration (Mohseni-Salehi et al., 2018), which is agreed with the larger crystalline size in the XRD results. The average pore

diameters of all catalysts measured by BET method are also shown in Table 1. The results disclosed that all prepared WO_3 catalysts have mesoporous structure. The smaller the average pore diameter, the larger the BET surface area.

Table 1. BET surface area of Bi/V/Mn oxide doped WO_3

Catalyst samples	BET surface area (m^2/g)	Average pore diameter (nm)
Undoped WO_3	18.2	11.6
0.5% (w/w) Bi_2O_3 doped WO_3	32.0	10.1
1% (w/w) Bi_2O_3 doped WO_3	29.2	10.5
2% (w/w) Bi_2O_3 doped WO_3	27.4	10.3
0.5% (w/w) V_2O_5 doped WO_3	24.3	12.0
1% (w/w) V_2O_5 doped WO_3	22.7	10.8
2% (w/w) V_2O_5 doped WO_3	19.3	11.2
0.5% (w/w) MnO_2 doped WO_3	22.5	12.1
1% (w/w) MnO_2 doped WO_3	20.8	12.0
2% (w/w) MnO_2 doped WO_3	19.5	12.0

XRD characterization from in Figure 2 showed the main characteristic peaks of Bi/V/Mn oxide doped WO_3 and undoped WO_3 corresponding to (002), (020), (200), (022), (222) and (400) planes. All the peaks of the prepared catalysts matched with standard monoclinic phase, which is an active phase of WO_3 (Hernandez-Uresti et al., 2014).

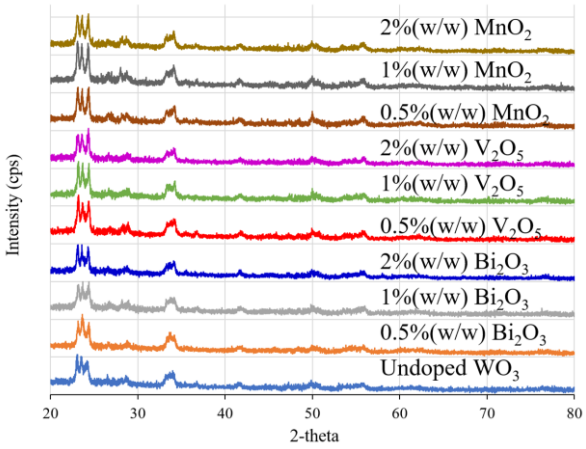

Figure 2. XRD patterns of Bi/V/Mn oxide doped WO_3

However, after doping metal oxide on WO_3, the main peaks showed the increase in crystalline size. It can be assumed that the metal oxide doped-WO_3 provide larger crystalline size than the undoped WO_3 and the increasing is due to alignment in the order of Bi>V>Mn, leading to suppression electrons-holes recombination (Concina and Vomiero, 2014; Xu et al., 2019). These results also confirmed with other research that an increase in crystalline size of WO_3 has strong influence in enhancing the photocatalytic degradation of organic compounds (Nandiyanto et al., 2020). According to the summary from XRD results in Table 2, the crystalline size of undoped and doped WO_3 were calculated based on Debye-Scherrer equation (Reddy et al., 2003) with the represented peak of (200).

Table 2. Crystalline size of Bi/V/Mn oxide doped WO_3 based on represented peak (200)

Catalyst samples	Crystalline size (nm)
Undoped WO_3	5.8
0.5% (w/w) Bi_2O_3 doped WO_3	13.2
1% (w/w) Bi_2O_3 doped WO_3	40.9
2% (w/w) Bi_2O_3 doped WO_3	37.2
0.5% (w/w) V_2O_5 doped WO_3	7.4
1% (w/w) V_2O_5 doped WO_3	30.8
2% (w/w) V_2O_5 doped WO_3	35.2
0.5% (w/w) MnO_2 doped WO_3	8.5
1% (w/w) MnO_2 doped WO_3	21.4
2% (w/w) MnO_2 doped WO_3	23.7

In Table 3, the calculated band gap energy form Kubelka-Munk (Lee et al., 2012) revealed that undoped WO_3 had the largest bandgap energy 2.8 eV whereas band gap energy of Bi/V/Mn oxide doped WO_3 was decreased with the increasing amount of metal oxide. The way the bandgap energy is minimized or decreased was aligned in the order, V>Bi>Mn. The 2% (w/w) V_2O_5 doped WO_3 possesses the lowest bandgap energy of 2.40 eV. Loading metal oxide brings about narrowing the band gap energy, driving more easily photodegradation under visible light region. However, more metal loading level could lead to increase in an electrons-holes recombination (Aware and Jadhav, 2016; Cimieri et al., 2013; Singla et al., 2014), which must be considered during the process.

Table 3. Band gap energy of Bi/V/Mn oxide doped WO_3

Catalyst samples	Band gap energy (eV)
Undoped WO_3	2.8
0.5% (w/w) Bi_2O_3 doped WO_3	2.58
1% (w/w) Bi_2O_3 doped WO_3	2.55
2% (w/w) Bi_2O_3 doped WO_3	2.52
0.5% (w/w) V_2O_5 doped WO_3	2.55
1% (w/w) V_2O_5 doped WO_3	2.49
2% (w/w) V_2O_5 doped WO_3	2.40
0.5% (w/w) MnO_2 doped WO_3	2.70
1% (w/w) MnO_2 doped WO_3	2.60
2% (w/w) MnO_2 doped WO_3	2.51

It is known that the photoluminescence spectrum reflects the electrons-holes recombination rate; the highest recombination rate belongs to an undoped WO_3 (Figure 3). However, the recombination rate decreased after doping Bi/V/Mn metal oxide, leading to improve in photocatalytic activity, which could be observed in the degradation results. This result agreed with the previous research that loading metal oxide on WO_3 would serve as impurities causing lattice defects, dominating the light absorption, and the separation of electron-hole pairs (Liu et al., 2018). The electrons and holes recombination have a

trade-off relationship with the band gap energy. When the band gap energy is narrow, the electrons-holes recombination rate will be higher (Kwong et al., 2013; Sachenko and Sokolovsky, 2007; Wei et al., 2013). The lowest electrons-holes recombination rate was found in 1% (w/w) Bi_2O_3 doped WO_3 with the highest the photocatalytic degradation of S-metolachlor under visible light removing 55.43% S-metolachlor and the highest reaction rate coefficient, calculated based on the pseudo first-order reaction. According to the XRF characterization, the doped metal oxide lost some small traces during sol-gel preparation, especially MnO_2, as shown in Table 4.

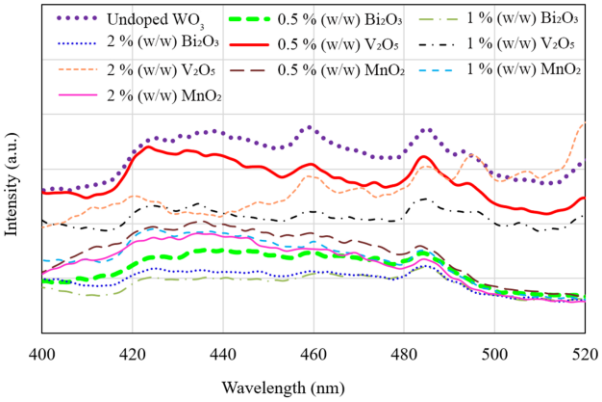

Figure 3. Photoluminescence spectrum of Bi/V/Mn oxide doped WO_3

Table 4. XRF of % (w/w) Bi/V/Mn oxide doped WO_3 based on 100% (w/w) WO_3

Catalyst samples	Percentage based on 100% (w/w) WO_3
1% (w/w) Bi_2O_3 doped WO_3	1.08
1% (w/w) V_2O_5 doped WO_3	1.29
1% (w/w) MnO_2 doped WO_3	0.85

3.2. The results of S-metolachlor photodegradation

The photocatalytic degradation of S-metolachlor using WO_3 and metal oxide doped WO_3 follows the pseudo first-order linear reaction (Long et al., 2014). The relationship between $-ln(C_A/C_{A0})$ and time is appeared to be linear. Hence, the reaction rate constant (k value) shown in Table 5 can be calculated from the Equation (2). Degradation rate of S-metolachlor is assumed to be equal to R_A,

$$R_A = -dC_A/dt \quad (1)$$

$$-ln(C_A/C_{A0}) = kt \quad (2)$$

while C_A is equal to the remaining concentration of S-metolachlor measured by UV-Vis, and C_{A0} is equal to an initial concentration of S-metolachlor.

Photocatalytic activities of degradation of S-metolachlor using different WO_3 catalysts under visible light are presented in Figure 4 based upon the remaining percentage of S-metolachlor as measured by UV-Vis spectroscopy. For 5-ppm initial concentration of S-metolachlor and 4-h retention time for the steady state, it was observed that using Bi_2O_3 doped WO_3 exhibited the highest degradation rate. Among other catalysts, 1% (w/w) Bi_2O_3 doped WO_3 had the highest photocatalytic activity which removed 55.43% S-metolachlor under visible light irradiation. This is similar to PL results, which provided the lowest electrons and holes recombination rate, as described in photoluminescence spectra in the previous section, and also possesses low energy bandgap with high BET surface area. Although 2% (w/w) Bi_2O_3 doped WO_3 had the lowest energy bandgap, its electrons and holes recombination rate was higher than 1% (w/w) Bi_2O_3 doped WO_3 (from PL results section). This is in agreement with theory that there is still some trade-off characteristic between bandgap energy and electrons and holes recombination rate (Kwong et al., 2013; Sachenko and Sokolovsky, 2007; Wei et al., 2013). Therefore, it can be assumed that the photocatalytic potential is significantly depended on three major factors in logical order: (1) electrons and holes recombination rate, (2) bandgap energy, and (3) BET surface area. The calculated reaction rate coefficient (k in unit of min^{-1}) is shown in the Table 5. According to the pseudo first-order reaction, the reaction rate coefficient progresses at a linear rate or depends on the reactant concentration. It is also observed that the highest reaction rate coefficient is possessed by 1% (w/w) Bi_2O_3 doped WO_3, which is equal to 0.0036 min^{-1}. These characteristics such as high surface area, low band gap energy, and the lowest electrons-holes recombination rate are similar to UV-Vis results, PL results, and BETresults, respectively.

Table 5. Reaction rate constant of Bi/V/Mn oxide doped and undoped WO_3 based on the assumption of the pseudo first-order reaction

Catalyst samples	Reaction rate constant (min^{-1})
Undoped WO_3	0.0010
0.5% (w/w)Bi_2O_3 doped WO_3	0.0029
1% (w/w)Bi_2O_3 doped WO_3	0.0036
2% (w/w)Bi_2O_3 doped WO_3	0.0029
0.5% (w/w) V_2O_5 doped WO_3	0.0017
1% (w/w)V_2O_5 doped WO_3	0.0018
2% (w/w)V_2O_5 doped WO_3	0.0019
0.5% (w/w)MnO_2 doped WO_3	0.0013
1% (w/w) MnO_2 doped WO_3	0.0017
2% (w/w)MnO_2 doped WO_3	0.0017

3.3. Reusability of doped WO_3

In order to test the catalyst reusability, the degradation experiment of S-metolachlor was repeated with the most active photocatalyst (1% (w/w) Bi_2O_3 doped WO_3) under visible light in three batches. The results are presented in Table 6. After each batch of S-metolachor photodegradation, the prepared WO_3 catalysts were then separated from the product solution using high speed microcentrifuge and left in the oven at 100°C for 3 h to remove the remaining moisture on catalysts surface prior to the further batch. According to Table 6, there was only slightly decrease in degradation percentage of S-metolachlor with the acceptable range of ±3%, which can be related to minimal catalyst deactivation.

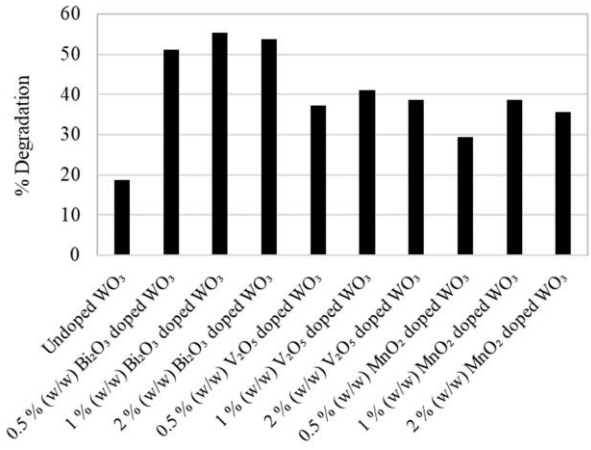

Figure 4. Degradation of S-metolachlor using Bi/V/Mn oxide doped WO_3 after 4 h under visible light

Table 6. Reusability of 1% (w/w) Bi_2O_3 doped WO_3

Catalyst samples	%S-metolachlor degradation
1st cycle	55.43
2nd cycle	53.14
3rd cycle	52.07

4. CONCLUSION

In this research, the influence of doping metals and loading amounts on the photocatalytic activity was studied for S-metolachlor degradation under visible light, and the characterization results of undoped WO_3 and Bi/V/Mn oxide doped WO_3 were obtained through XRD, XRF, UV-Vis, BET, and PL. Among several factors, the electrons-holes recombination rate would be the strongest influencing factor on developing the catalytic activity of WO_3, which a trade-off characteristic with the band gap energy. The most interesting finding is that PL results showed that 1% (w/w) Bi_2O_3 doped WO_3 possesses the lowest electrons and holes recombination rate, which corresponds to the highest degradation rate and highest degradation percentage of S-metolachlor at 55.43% under visible light The undoped WO_3 provided merely 18.78% S-metolachlor degradation. When considering other factors, the lowest bandgap energy of 2.40 eV was found in 2% (w/w) V_2O_5 doped WO_3. The BET largest surface area of 32 m^2/g was observed in the low metal oxide loading amount of 0.5% (w/w) MnO_2 doped WO_3. After using 1% (w/w) Bi_2O_3 for doping WO_3 for few cycles in the S-metolachlor degradation, there is an insignificant drop in catalytic performance since there was only slightly decrease in degradation percentage of S-metolachlor with an acceptable range of ±3%.

REFERENCES

Aware, V. D., and Jadhav, S. S. (2016). Synthesis, characterization and photocatalytic applications of Zn-doped TiO_2 nanoparticles by sol-gel method. *Applied Nanoscience*, 7(6), 965-972.

Badawy, M. I., Ghaly, M. Y., and Gad-Allah, T. A. (2006). Advanced oxidation processes for the removal of organophosphorus pesticides from wastewater. *Desalination*, 194 (1-3), 166-175.

Cimieri, L., Poelman, H., Ryckaert, J., and Poelman, D. (2013). Novel sol-gel preparation of V-TiO_2 films for the photocatalytic oxidation of ethanol in air. *Journal of Photochemistry and Photobiology A: Chemistry,* 263(1), 1-7.

Concina, I., and Vomiero, A. (2014). Metal oxide semiconductors for dye- and quantum-dot sensitized solar cells. *Small*, 11(15), 1744-1774.

Fraga, L. E., Franco, J. H., Orlandi, M. O., and Zanoni, M. V. B. (2013). Photoelectrocatalytic oxidation of hair dye basic red 51 at W/WO_3/TiO_2 bicomposite photoanode activated by ultraviolet and visible radiation. *Journal of Environmental Chemical Engineer*, 1(3), 194-199.

Hernandez-Uresti, D. B., Sánchez-Martínez, D., La Cruz, A. M.-D., Sepúlveda-Guzmán, S., and Torres-Martínez, L. M. (2014). Characterization and photocatalytic properties of hexagonal and monoclinic WO_3 prepared via microwave-assisted hydrothermal synthesis. *Ceramics International*, 40(3), 4767-4775.

Kwong, W. L., Qiu, H., Nakarak, A., Koshy, P., and Sorrell, C. C. (2013). Photoelectrochemical properties of WO_3 thin films prepared by electrodeposition. *Energy Procedia*, 34, 617-626.

Laoufi, N. A., and Bentahar, F. (2014). Pesticide removal from water suspension by UV/ TiO_2 process: a parametric study. *Desalination and Water Treatment*, 52(10-12), 1947-1955.

Lee, J. S., You, H. K., and Park, C. B. (2012). Highly photoactive, low bandgap TiO_2 nanoparticles wrapped by graphene. *Advanced Materials*, 24(8), 1084-1088.

Liu, Q., Wang, F., Lin, H., Xie, Y., Tong, N., Lin, J., Zhang, X., Zhang, Z., and Wang, X. (2018). Surface oxygen vacancy and defect engineering of WO_3 for improved visible light photocatalytic performance. *Catalysis Science and Technology*, 8(17), 4399-4406.

Long, Y. H., Li, R. T., and Wu, X. M. (2014). Degradation of S-metolachlor in soil as affected by environmental factors. *Journal of Soil Science and Plant Nutrition*, 14(1), 189-198.

Mohseni-Salehi, M. S., Taheri-Nassaj, E., and Hosseini-Zori, M. (2018). Effect of dopant (Co, Ni) concentration and hydroxyapatite compositing on photocatalytic activity of titania towards dye degradation. *Journal of Photochemistry and Photobiology A: Chemistry*, 365(1), 57-70.

Nandiyanto, A. B. D., Zaen, R., and Oktiani, R. (2020). Correlation between crystallite size and photocatalytic performance of micrometer-sized monoclinic WO_3 particles. *Arabian Journal of Chemistry*, 13(1), 1283-1296.

Reddy, K. M., Manorama, S. V., and Reddy, A. R. (2003). Bandgap studies on anatase titanium dioxide nanoparticles. *Materials Chemistry and Physics,* 78(1), 239-245.

Rosenfield, P. E., and Feng, L. G. H., (2011). *Risks of Hazardous Wastes*, 1st, Elsevier Publishing Ltd., pp. 127-154.

Sachenko, A. V., and Sokolovsky, I. O. (2007). The effect of narrowing of the band gap on surface recombination in silicon. *Semiconductors*, 41(6), 673-678.

Singla, P., Sharma, M., Pandey, O. P., and Singh, K. (2014). Photocatalytic degradation of azo dyes using Zn-doped and undoped TiO_2 nanoparticles. *Applied Physics A*, 116(1), 371-378.

Susanti, D., Diputra, A. A. G. P., Tananta, L., Purwaningsih, H., Kusuma, G. E., Wang, C., Shih, S., and Huang, Y. (2014). WO_3 nanomaterial synthesized via a sol-gel

method and calcination for use as a CO gas sensor. *Frontiers of Chemical Science and Engineering*, 8(2), 179-187.

Wang, S. H., Chou, T. C., and Liu, C. C. (2003). Nano-crystalline tungsten oxide NO_2 sensor. *Sensors and Actuators B: Chemical*, 94(3), 343-351.

Wei, W. D., Duchene, J. S., Sweeny, B. C., Wang, J., and Niu, W. (2013). Current development of photocatalysts for solar energy conversion, new and future developments in catalysis. In *New and Future Developments in Catalysis* (Suib, S. L. ed.), pp. 279-304. Amsterdam, Elsevier.

Xu, Y., Liu, J., Cui, Y., Yin, R., Wang, X., Wu, S., and Yu, X. (2019). Efficient polycrystalline silicon solar cells with double metal oxide layers. *Dalton Transactions*, 48(11), 3687-3694.